Absence of the hyperfine magnetic field at the Ru site in ferromagnetic rare-earth intermetallics

D. Coffey
Department of Physics, Buffalo State College, Buffalo, New York 14222, USA

M. DeMarco
Department of Physics, Buffalo State College, Buffalo, New York 14222, USA
and Department of Physics, SUNY–Buffalo, Buffalo, New York 14260, USA

P. C. Ho
Department of Physics, California State, Fresno, California 93740, USA

M. B. Maple and T. Sayles
Department of Physics, University of California, San Diego, California 92093, USA

J. W. Lynn and Q. Huang
NIST Center for Neutron Research, National Institute of Standards and Technology, Gaithersburg, Maryland 20899, USA

S. Toorongian and M. Haka
Nuclear Medicine Department, State University of New York, Buffalo, New York 14260, USA
(Received 13 October 2009; revised manuscript received 29 March 2010; published 3 May 2010)

The Mössbauer effect (ME) is frequently used to investigate magnetically ordered systems. One usually assumes that the magnetic order induces a hyperfine magnetic field, $B_{hyperfine}$, at the ME active site. This is the case in the ruthenates, where the temperature dependence of $B_{hyperfine}$ at ^{99}Ru sites tracks the temperature dependence of the ferromagnetic or antiferromagnetic order. However this does not happen in the rare-earth intermetallics, $GdRu_2$ and $HoRu_2$. Specific heat, magnetization, magnetic susceptibility, Mössbauer effect, and neutron diffraction have been used to study the nature of the magnetic order in these materials. Both materials are found to order ferromagnetically at 83.1 and 15.3 K, respectively. Despite the ferromagnetic order of the rare-earth moments in both systems, there is no evidence of a correspondingly large $B_{hyperfine}$ in the Mössbauer spectrum at the Ru site. Instead the measured spectra consist of a narrow peak at all temperatures which points to the absence of magnetic order. To understand the surprising absence of a transferred hyperfine magnetic field, we carried out *ab initio* calculations which show that spin polarization is present only on the rare-earth site. The electron spin at the Ru sites is effectively unpolarized and, as a result, $B_{hyperfine}$ is very small at those sites. This occurs because the 4*d* Ru electrons form broad conduction bands rather than localized moments. These 4*d* conduction bands are polarized in the region of the Fermi energy and mediate the interaction between the localized rare-earth moments.

DOI: 10.1103/PhysRevB.81.184404 PACS number(s): 76.80.+y, 71.20.Lp, 28.20.Cz, 75.50.Cc

I. INTRODUCTION

Compton and Matthias[1] found that superconductivity and ferromagnetism occur in Laves phase compounds containing lanthanide elements and Ru. This led to the suggestion that superconductivity and ferromagnetism could coexist in $Ce_{1-x}Gd_xRu_2$ alloys, since superconductivity occurs below 6 K in $CeRu_2$ and ferromagnetism is present above 70 K in $GdRu_2$.[2] $CeRu_2$ has the cubic Laves structure ($Fd\bar{3}m$), although recently Huxley *et al.*[3] have shown that its symmetry is lowered due to a slight variation in the displacement of the Ru from their cubic Laves positions. $GdRu_2$ and $HoRu_2$ have the hexagonal Laves phase structure ($P6_3/mmc$). $GdRu_2$ has also been reported in the cubic Laves phase.[4] The difference in structure does not determine whether the ground state is superconducting or ferromagnetic since $NdRu_2$ and $PrRu_2$, both ferromagnets, have the $Fd\bar{3}m$ structure.

The phase diagram for $Ce_{1-x}R_xRu_2$ was investigated by Wilhelm and Hillebrand[5] for R=Gd, Ho, Dy, and Pr. No long range magnetic order was found in the superconducting region of the phase diagrams of these alloys. However evidence for short-range order was found in the temperature dependence of the ^{155}Gd Mössbauer effect (ME) and in nuclear quadrupole resonance measurements for a narrow range of doping about $x \sim 0.1$ in $Ce_{1-x}Gd_xRu_2$.[6,7] Fischer and Peter[8,9] pointed out that the specific heat of $Ce_{1-x}Gd_xRu_2$ also showed an anomalous temperature dependence. The specific heat divided by temperature, $\frac{C}{T}$, for $CeRu_2$ showed a sharp jump at the superconducting transition and a rapid fall off to zero as $T \rightarrow 0$, as expected. However the jump becomes more rounded in $Ce_{1-x}Gd_xRu_2$ as x increases from 0.05 to 0.11 and $\frac{C}{T}$ increases as $T \rightarrow 0$. This anomalous temperature dependence was taken as evidence of a ferromagnetic contribution to $\frac{C}{T}$. The analysis of the data did not provide a microscopic model for the nature of this contribution or explain how it could coexist with superconductivity.

Evidence for the coexistence of superconductivity and short-range ferromagnetic correlations was also found in

$Ce_{0.73}Ho_{0.27}Ru_2$ from the temperature dependence of the ^{57}Fe ME below ~2 K and from neutron-scattering data.[10–12] Since the hyperfine coupling constant of Ru is twice that of Fe,[13] it was expected that there would be a magnetic field at the Ru nucleus of about 15 T in this material. Hyperfine magnetic fields ($B_{hyperfine}$) were reported at the Gd site in $Ce_{1-x}Gd_xRu_2$ (Ref. 6) for $x>0.1$, whose temperature dependence was consistent with the Curie temperature.

The present work was motivated by a search for evidence of coexisting ferromagnetism and superconductivity in $Ce_{1-x}Gd_xRu_2$ using the ^{99}Ru ME. Mössbauer spectroscopy is a nuclear probe of the electronic properties of systems which has been used to investigate magnetic order in many systems. The evidence of magnetic order appears in the Mössbauer spectrum as a hyperfine magnetic field induced at the nucleus at which the ME is measured. In this way the temperature dependence of magnetic order has been probed by the ^{99}Ru ME in both ferromagnetic and antiferromagnetic ruthenates.[14,15] As the Gd content of $Ce_{1-x}Gd_xRu_2$ increases with increasing x, T_{SC} falls and goes to zero at $x \simeq 0.14$. Our measured spectra of $Ce_{0.88}Gd_{0.12}Ru_2$ at 2.2, 4.2, and 17 K show no evidence for a hyperfine magnetic field, suggesting that ferromagnetism is ruled out at this doping. However, as doping with Gd increases, the low temperature phase is known to be ferromagnetically ordered and, at $x=0.2$, one would expect to see an eighteen line magnetic spectrum at 4.2 K due to a large value of $B_{hyperfine}$ field at the Ru site. However a hyperfine magnetic field is absent even in this sample.

The magnetic order in the intermetallic compounds of interest here has also been investigated using the ^{57}Fe, ^{193}Ir, and ^{155}Gd ME. One can distinguish between two cases. In the first case the $B_{hyperfine}$ is found at a site on which there is an ordered electronic moment. This is the case of the ruthenates and a number of rare-earth intermetallics. Using the ^{57}Fe ME, Wertheim and Wernick[16] measured $B_{hyperfine}$ values in RFe_2(R=Ce,Sm,Gd,Dy,Ho,Er,Tm). $B_{hyperfine}$ is found to be ~23 T in spite of the wide range in the size of the localized moments on the R sites. By comparison, the value for $B_{hyperfine}$ in ferromagnetic Fe is 33 T. The ^{57}Fe ME has also been used to investigate the magnetic structure in rare-earth iron ternary intermetallics.[17] De Graaf *et al.*[18] extracted a value for $B_{hyperfine}$ equal to 17.5 T at the Gd site in $GdCu_2$ using ^{155}Gd ME from a structureless spectrum.

In the second case, for a nonmagnetic ion in a magnetically ordered lattice, the measured ME at this site is expected to show evidence of the magnetic order through a transferred hyperfine magnetic field. Kistner measured a 50 T transferred hyperfine magnetic field at the Ru site in $Ru_{0.023}Fe_{0.977}$.[19] Transferred hyperfine fields at the nonmagnetic Ir site in RIr_2(R=Pr,Nd,Sm,Gd,Tb,Dy,Ho) were measured by Atzmony *et al.*[20] They found a wide variation from 4 T in $HoIr_2$ to 19 T in $GdIr_2$. Transferred hyperfine fields have also been measured in a rare-earth matrix doped with 1% Sn and in R_2Sn using the ^{119}Sn ME.[21] For Sn doped into a rare-earth, these range from −5.3 T in a Tm matrix to 23.8 T in a Gd matrix. The values of $B_{hyperfine}$ are linear in the projection of the spin of the rare-earth moment on its total angular momentum. In R_2Sn, these fields range from −5.5 T(Er_2Sn) to 28.9 T (Gd_2Sn).

The fact that the sign of the transferred hyperfine field can change suggests that there is competition between different contributions which align or antialign the nuclear moment with the ordered electronic moment. A negative hyperfine magnetic field is antiparallel to the ordered electronic moment. Watson and Freeman were among the first to investigate the origin of the hyperfine magnetic field with large scale numerical calculations based on the Hartree-Fock approximation.[22,23] Although these calculations were limited by the computational capabilities then available, they demonstrated a number of the qualitative features of the experimental data. In particular, they showed that the ordered $4f$ moment in Gd polarizes the electron density in the opposite direction to the ordered $4f$ moment both very close to the nucleus and in the region beyond ~1 Å from the Gd nucleus. They showed that the largest contribution to the hyperfine magnetic field due to polarization of the spin density of s electrons is the result of contributions of different signs from different s shells. Their calculations also showed that the polarization of the spin density on neighboring sites could be opposite to that of the ordered moments leading to the negative hyperfine magnetic field. The sign of the transferred hyperfine field can be modulated by varying the lattice constant, as we describe in the section on calculations of the electronic properties below. In the calculations of Watson and co-workers, it was assumed that the $5s$ electrons formed the conduction band which turns out not to be the case in $GdRu_2$, as we will also discuss below. In addition orbital contributions to transferred hyperfine magnetic field, based on the assumption that it arises from the coupling of f electrons on the rare-earth sites with s conduction electrons, were investigated by Dunlap *et al.*[24] Local spin density approximation (LSDA) calculations were first used to calculate hyperfine magnetic fields in ferromagnetic $3d$ metals by Callaway and Wang.[25,26]

The absence of evidence for magnetic order in the ^{99}Ru ME in $Ce_{0.2}Gd_{0.8}Ru_2$ led us to investigate the properties of $GdRu_2$ and $HoRu_2$. We present magnetic, transport, and thermodynamic data on $GdRu_2$, and magnetic and neutron diffraction data on $HoRu_2$, showing that these are ferromagnetically ordered at low temperatures. However, our ME measurements of $GdRu_2$ and $HoRu_2$ show that $B_{hyperfine}$ at the Ru site is so small that, without the evidence of other experiments, one would conclude that there is no magnetic order. The absence of $B_{hyperfine}$ is an unexpected result in $GdRu_2$ and $HoRu_2$ whose Curie temperatures determined here are 83.1 and 15.3 K, respectively, although it is consistent with the measured spectrum of $Ce_{0.2}Gd_{0.8}Ru_2$. Interestingly, the absence of $B_{hyperfine}$ at the Ru sites in $GdRu_2$ was noted previously.[19]

We calculate the electronic properties of these materials using a spin polarized fully relativistic all-electron linearized augmented plane-wave method.[27] *Ab initio* band-structure calculations have previously been used by other authors to determine hyperfine magnetic fields and electric field gradients (EFG).[28–31] We find that the calculated $B_{hyperfine}$ at the Ru sites in $GdRu_2$ and $HoRu_2$ are much smaller than those on Gd and Ho, consistent with the experimental results. First we present the experimental results.

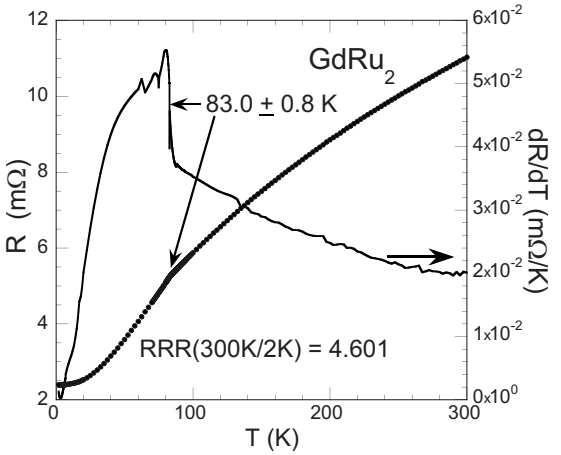

FIG. 1. Temperature T dependence of resistance R and the slope dR/dT of a polycrystalline sample of $GdRu_2$. The value of the residual resistivity ratio RRR (300K/2K) is ~4.6. A curvature breaking occurs in the $R(T)$ data at 83.0 ± 0.8 K corresponds to the transition temperature of magnetic order.

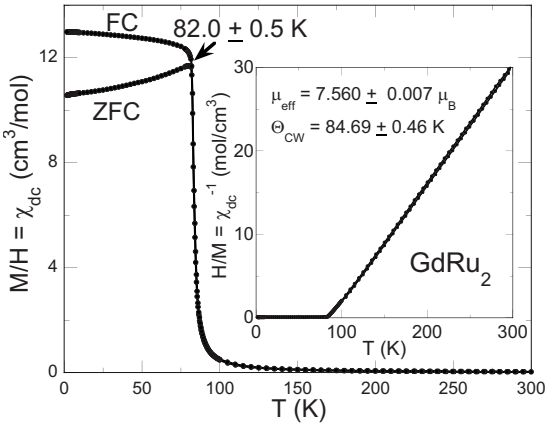

FIG. 2. Temperature dependence of dc magnetic susceptibility χ_{dc} of $GdRu_2$ measured at an applied magnetic field $H=50$ Oe. A hysteresis occurs at $T=82.0\pm0.5$ K, coinciding with the Curie temperature T_C determined from the modified Arrott plot analysis (83.1 ± 2.3 K, displayed in Fig. 3). Inset χ_{dc}^{-1} vs T fits well with a Curie-Weiss behavior, which results in an effective moment $\mu_{eff}=7.560\pm0.007\mu_B$ and a Curie-Weiss temperature $\Theta_{CW}=84.69\pm0.46$ K.

II. EXPERIMENTAL TECHNIQUES

A. Sample preparation and characterization

Polycrystalline samples of RRu_2 (R=Gd and Ho) were prepared in a single arc furnace by using the stoichiometric ratio of the elements R: Ru=1: 2. In order to ensure the uniform formation of an alloy, each ingot was arced, flipped over, and arced again six times. Then the ingot was removed from the arc furnace, cracked into small pieces, and examined under a microscope for homogeneous coloration as an indication of homogeneity. If the color is not uniform, the ingot was resealed in the arc furnace and the arc melting process repeated. During this process, mass loss can occur due to the low vapor pressure of the rare-earth elements. In order to ensure the correct stoichiometric ratio, the effective moment from the Curie Weiss analysis of the dc magnetic susceptibility data of the sample boule is used to check how much mass of the rare-earth is needed to compensate for the loss during arc melting. Up to 3% of the original mass of Gd was needed. We found that there was no significant mass loss in the case of Ho. A small piece of the final product was taken to be powdered for a x-ray diffraction measurement performed in Rigaku D/MAX B x-ray machine. The $HoRu_2$ and $GdRu_2$ samples were confirmed to have a $MgZn_2$ crystalline structure ($P6_3/mmc$) and to have a single phase.

Measurements of electrical resistance (standard four-wire technique) and specific heat (1-τ relaxation method) were made in a quantum design physical property measurement system. Magnetic susceptibility and magnetization measurements were performed in a SQUID magnetometer (quantum design magnetic property measurement system).

B. Neutron scattering

High-resolution powder diffraction data were collected at the NCNR on the BT-1 high-resolution neutron powder diffractometer on the $HoRu_2$ sample, using monochromatic neutrons of wavelength 1.5403 Å produced by a Cu(311) monochromator. Söller collimations before and after the monochromator and after the sample were 15′, 20′, and 7′ full width at half maximum (FWHM), respectively. Data were collected in the θ range of 3° to 168° with a step size of 0.05° at 25 and 5 K, above and below the magnetic phase transition. Structural refinements were carried out using the GSAS program.[32]

Detailed temperature dependent measurements of the magnetic order parameter were carried out on the BT9 triple axis spectrometer. A pyrolytic graphite (PG) (002) monochromator was employed to provide neutrons of wavelength 2.36 Å, and a PG filter was used to suppress higher-order wavelength contaminations. Coarse collimations of 40′, 48′, and 40′ FWHM on BT9 were employed to maximize the intensity. A PG(002) energy analyzer was used in these measurements. Inelastic measurements were taken on BT7 with a fixed final energy of 14.7 meV.

C. Mössbauer effect measurements

^{99}Ru Mössbauer spectroscopy was performed using a 5 mCi ^{99}Rh (Ru) source prepared at the University at Buffalo cyclotron by (p,xn) reactions on enriched ^{100}Ru and ^{101}Ru with 30 MeV protons. The calibration for the velocity was found by using the inner four lines of the ^{57}Fe Mössbauer spectrum. The sample holder is made of aluminum with a top and bottom piece. The bottom or "window" of the holder is 0.04 cm thick with an area of 1.5 cm^2. A thin aluminum plonger was used at the top of the holder to clamp the powder in place. Since Gd and Ho both absorb the 90 keV Mössbauer gamma ray, it was found necessary to use enriched ^{99}Ru (95%) samples of $GdRu_2$ and $HoRu_2$ to obtain well-resolved spectra at low temperatures and particularly at higher temperatures. Typical samples contained 65 mg/cm^2 ^{99}Ru. Both samples and source were in close proximity inside the sample chamber in a vertical cryostat which used an

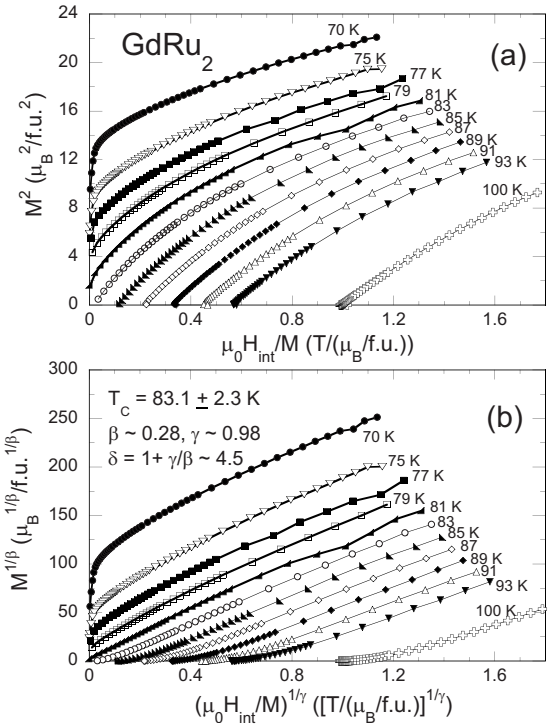

FIG. 3. (a) Conventional and (b) modified Arrott plots of $GdRu_2$. Curie temperature T_C of $GdRu_2$ determined from the analysis of the modified Arrott plot is 83.1 ± 2.3 K. Ferromagnetism in $GdRu_2$ slightly deviated from to the mean-field type, which may be due to disorder in the unannealed sample of $GdRu_2$.

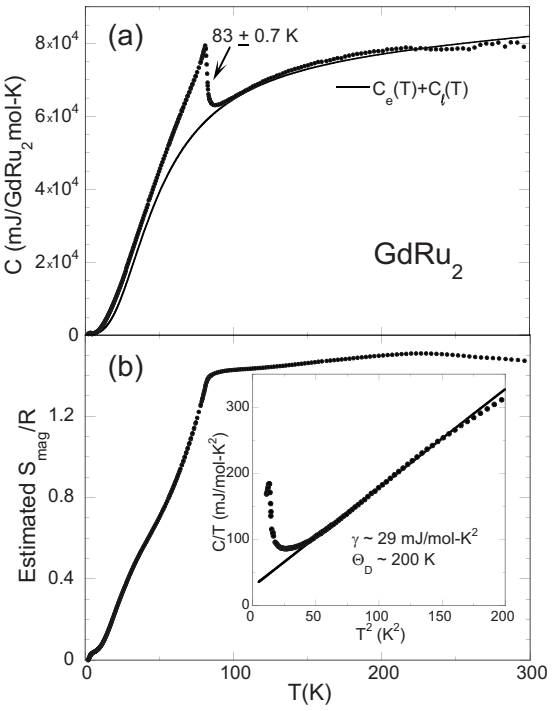

FIG. 4. (a) Specific heat C vs temperature T of $GdRu_2$. A specific-heat jump occurs at 83.0 ± 0.7 K, corresponding to the ferromagnetic ordering temperature determined from other measurements. The solid line is the sum of the estimated contribution from electrons and phonons $C_e(T)+C_\ell(T)$. Inset of (b) C/T vs T^2 below 14 K. The estimated values of electronic specific heat coefficient γ and Debye temperature Θ_D are ~29 mJ/mol-K^2 and ~200 K, respectively. (b) Estimated magnetic entropy S_{mag} of $GdRu_2$ after the contribution from electron and lattice is removed. The saturation value of S_{mag} is ~1.5 R, less than R ln 8.

exchange gas for both heating and cooling. Gamma rays were detected using 0.25-inch-thick NaI detector below the cryostat. Measurements at higher temperature were accomplished by using a heating wire on the samples and a Lake-Shore temperature controller which controlled temperatures to better than 1 K using a diode thermometer on the sample.

III. EXPERIMENTAL RESULTS

A. Evidence of ferromagnetism

In this section, we demonstrate that ferromagnetoc order occurs in $GdRu_2$ and $HoRu_2$ from magnetic susceptibility, specific heat, transport, and neutron-scattering data. The transport and thermodynamic properties of an unannealed sample of $GdRu_2$ were investigated with a number of probes. The temperature, T, dependence of electrical resistance, R, and the slope dR/dT of a polycrystalline sample of $GdRu_2$ are plotted in Fig. 1. A breaking curvature in R, accompanied by a sharp increase of dR/dT, occurs at 83.0 ± 0.8 K as temperature decreases, which is due to the development of an ordered state. The dc magnetic susceptibility χ_{dc} is measured from 1.9 to 300 K at an applied magnetic field $H=50$ Oe in the zero-field cooled (ZFC) and field cooled (FC) states and the data are displayed in Fig. 2. Hysteresis in $\chi_{dc}(T)$ appears at 82.0 ± 0.5 K. A Curie-Weiss analysis was done on the molar magnetic susceptibility data χ_{mol} given by

$$\chi_{mol} = \frac{1}{3} \frac{N_A \mu_{eff}^2}{k_B (T - \Theta_{CW})}, \quad (1)$$

where N_A is the Avogadro's number, $\mu_{eff} = g(JLS)\sqrt{J(J+1)}\mu_B$ is the effective magnetic moment, $g(JLS)$ is the Landé g factor, k_B is the Boltzmann's constant, and Θ_{CW} is the Curie-Weiss temperature. A positive $\Theta_{CW} = 84.7 \pm 0.5$ K indicates ferromagnetic order in $GdRu_2$ and $\mu_{eff} = 7.56 \pm .007$ μ_B (Bohr magneton), which is close to the theoretical value (≈ 7.94 μ_B of the free-ion moment of Gd^{3+}). This value of Θ_{CW} is consistent with the temperature at which hysteresis first appears.

Because Gd has a large cross-section for neutron capture, neutron-scattering measurements to determine the ferromagnetic ordering temperature are impractical. Therefore, Arrott plots of magnetization M with respect to the internal magnetic flux density $\mu_0 H_{int}$ divided by M were constructed in an attempt to determine the Curie temperature T_C more accurately. A conventional Arrott plot consisting of M^2 vs $(\mu_0 H_{int}/M)$ isotherms, is shown in Fig. 3(a). In the simplest mean-field analysis of ferromagnetism, M^2 vs $(\mu_0 H_{int}/M)$ isotherms form a series of parallel straight lines near T_C, and the isotherm passing through the origin corresponds to T_C. However, the M^2-$(\mu_0 H_{int}/M)$ isotherms of $GdRu_2$ are

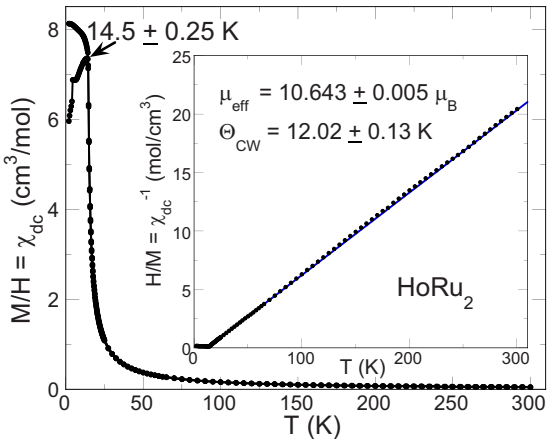

FIG. 5. (Color online) Temperature dependence of dc magnetic susceptibility χ_{dc} of $HoRu_2$ measured at an applied magnetic field $H=100$ Oe. A hysteresis occurs at $T\sim14.5$ K. Inset χ_{dc}^{-1} vs T fits well with a Curie-Weiss behavior, which results in an effective moment $\mu_{eff}=10.643\pm0.005$ μ_B and a Curie-Weiss temperature $\Theta_{CW}=12.02\pm0.13$ K.

slightly curved. Therefore, we applied a modified Arrott plot $M^{1/\beta}$ vs $(\mu_0 H_{int}/M)^{1/\gamma}$, where $\beta\sim0.28$ and $\gamma\sim0.98$ are the critical exponents based on the Arrott-Noakes equation,[33] and the results are plotted in Fig. 3(b). The value of T_C is 83.1 ± 2.3 K.

Figure 4(a) shows the specific heat C of $GdRu_2$ from 2 to 300 K. As T decreases to 83.0 ± 0.7 K, C starts to rise and peaks at ~81 K, indicating the bulk nature of the ferromagnetic second order phase transition. From the C/T vs T^2 analysis between 7 and 14 K [inset of Fig. 4(b)], the values of the electronic specific coefficient γ and the Debye temperature Θ_D of $GdRu_2$ are estimated to be 29 mJ/mol-K, and 200 K, which seem reasonable in comparison with $LaRu_2$'s $\gamma\sim41.6$ mJ/mol-K and $\Theta_D\sim158.4$ K.[34] After subtraction of electron and phonon contributions $C_e(T)+C_\ell(T)$ from $C(T)$ [Fig. 4(a)], the temperature dependence of the estimated magnetic entropy S_{mag} is displayed in Fig. 4(b). Estimated S_{mag} reaches a saturated value of 1.5 R above T_C which is lower than the expected value of R ln 8 (≈2 R). This could be due to a temperature dependent Θ_D of $GdRu_2$ or our overestimate for the phonon contribution to the specific heat.

Measurements of χ_{dc}, performed on $HoRu_2$ at $H=100$ Oe and from 2 to 300 K in the ZFC and FC conditions, are displayed in Fig. 5. Hysteresis in $\chi_{dc}(T)$ occurs at ~14.5 K. The Curie-Weiss analysis (shown in the inset of Fig. 5) indicates a ferromagnetic transition takes place near $\Theta_{CW}=12.02\pm0.13$ K in $HoRu_2$ with a $\mu_{eff}=10.643\pm.005$ μ_B, which agrees with the theoretical value ≈10.6 μ_B of the free-ion moment of Ho^{3+}. The hysteresis between the ZFC and FC χ_{dc} data shows a difference of 20% at 2 K n $HoRu_2$ compared with ~13% difference in $GdRu_2$, Fig. 2).

Figure 6 shows the diffraction pattern obtained above (25 K) and below (4 K) the magnetic transition. The diffuse background scattering in the magnetically disordered state is due to paramagnetic scattering of the uncorrelated Ho moments, which decreases with increasing angle due to the

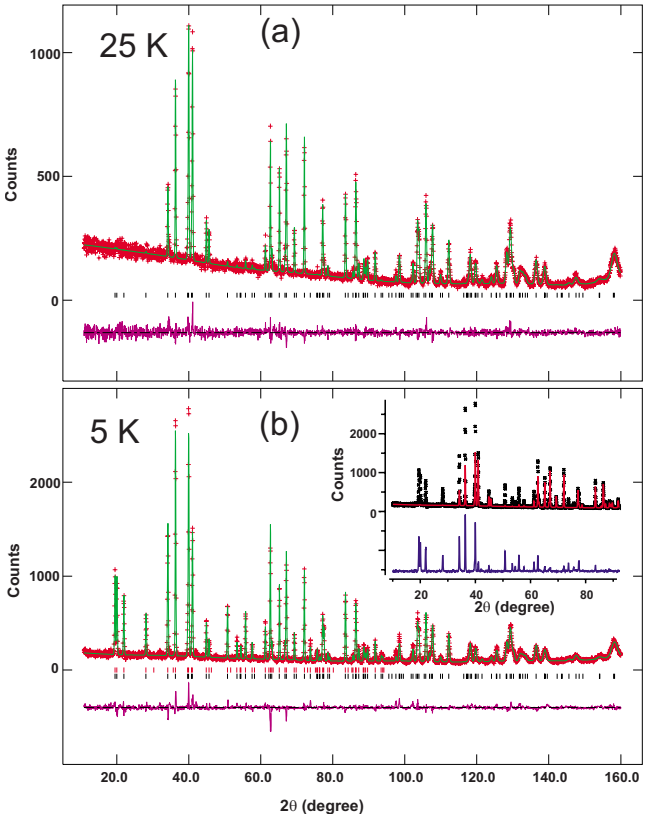

FIG. 6. (Color online) High-resolution neutron diffraction patterns for $HoRu_2$ taken (a) above and (b) below the magnetic phase transition at 15.3 K as determined by the temperature dependence of the magnetic Bragg intensity. The crosses indicate the observed data and the solid curves the calculated intensities from the structural refinements, and the difference is shown in the low part of the plots. The vertical lines indicate the angular positions of the diffraction lines for the nuclear Bragg peaks and (b) for the magnetic (top) Bragg peaks.

magnetic form factor. The overall refinement fits at both temperatures are excellent. No evidence of any impurity phase peaks was found to a sensitivity of <0.5%, indicating that the sample is single phase. The structure is found to deviate slightly from the ideal phase, and the refined values for the crystal structure are given in Table I. In the ground state the Ho ions exhibit long range ferromagnetic order with both in-plane and c-axis components of the ordered moment also given in Table I. We find an ordered moment of $7.98(8)\mu_B$, which is in good agreement with the low-temperature magnetization data of Andoh (Ref. 35) and somewhat smaller than the Curie-Weiss value obtained from the magnetization measurements. No evidence was found for moments on the Ru sites. The crystal and magnetic structures are shown in Fig. 7.

The temperature dependence of the magnetic Bragg intensity, which is proportional to the square of the ordered magnetic moment, is shown in Fig. 8. The temperature dependence is smooth and typical for magnetic ordering, and the solid curve is least-squares fit of the intensity to a mean field order parameter, which provides a good fit to the data with a Curie temperature of 15.30(4) K.

TABLE I. Refined crystal structure parameters for $HoRu_2$ at 25 K (first line) and 5 K (second line) space group $P6/3mmc$ (No. 194) a=5.2310(2)(Å), c=8.8265(4)(Å), and V=209.16(2)(Å^3).

Atom	x	y	z	B (Å^2)	M_x (μ_B)	M_z (μ_B)	M (μ_B)
Ho	1/3	2/3	0.0664(2)	0.36(3)			
	1/3	2/3	0.0660(2)	0.03(3)	6.70(8)	4.3(1)	7.98(8)
Ru_1	0	0	0	0.39(3)			
	0	0	0	0.22(3)			
Ru_2	0.1704(2)	0.3407(2)	3/4	0.39(3)			
	0.1711(2)	0.3422(4)	3/4	0.22(3)			
	Rp=6.16%, 7.12		wRp=7.34%, 9.02			χ^2=0.8387 1.428	

The diffraction data indicate that the ordered moment is reduced from the free-ion value of 10.0 μ_B and the value found from the fit to χ_{dc}^{-1}, which suggests that crystal field effects are important in this system at low temperatures. We therefore carried out inelastic neutron scattering measurements on BT-7 for several temperatures and wave vectors to search for crystal-field excitations. Figure 9 shows a scan above the phase transition, at a temperature of 20 K. We see two clear excitations from the crystal field ground state, a strong one at 2.83(5) meV and a weaker excitation at 14.82(5) meV. The energies and intensities turn out to be quite similar to the Ho crystal field levels observed in the closely related $Ce_{1-x}Ho_xRu_2$ system for smaller x,[10,11] which has the cubic C-15 Laves structure. The rare-earth site symmetry in the $CeRu_2$ case is cubic, $\bar{4}3m$, and the crystal-field level scheme has been worked out in detail. For hexagonal $HoRu_2$ the site symmetry is lower, $3m$, but the crystal field-levels look remarkably similar nevertheless. As we will show below, this is consistent with the calculated electric-field gradients which indicate only a modest deviation from cubic symmetry. The width for the higher energy level is limited by the instrumental resolution, while the level at 2.83 meV has an observed FWHM of 4.34(12) meV, which is much broader than the resolution of 1.5 meV. The width likely originates from exchange broadening. We note that both excitations are clearly magnetic in origin, as their intensity decreases with increasing wave vector, following the magnetic form factor dependence, and they decrease in intensity with increasing temperature as the ground-state occupancy is depleted.

All the thermodynamic, transport, neutron diffraction measurements clearly demonstrate that ferromagnetic order develops in $GdRu_2$ below 83 K and in $HoRu_2$ below 15 K.

B. ^{99}Ru Mössbauer spectra

The Mössbauer spectrum for $GdRu_2$ is an almost temperature independent single peak between 4.2 and 101 K except for a shift toward more positive velocities and a slightly increasing linewidth with increasing temperature. This is shown in Fig. 10 for 4.2 and 78 K, where the 78 K spectrum is scaled by 3 to compensate for the temperature dependence of the recoil free fraction so that a direct comparison can be made with the 4.2 K spectrum. The experimental FWHM of the spectrum is slightly broader than that of Ru powder (0.25 mm/s). This is also the case for the spectra at 89 and 101 K

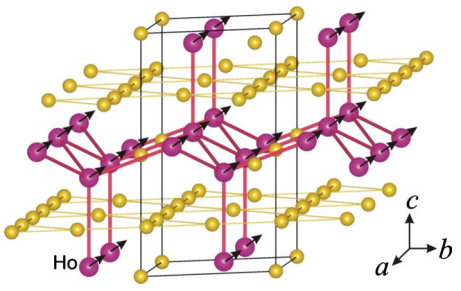

FIG. 7. (Color online) The hexagonal laves phase and magnetic structure of $HoRu_2$ at 5 K. The ferromagnetically ordered moments on the Ho sites have a magnitude of 7.98(8)μ_B.

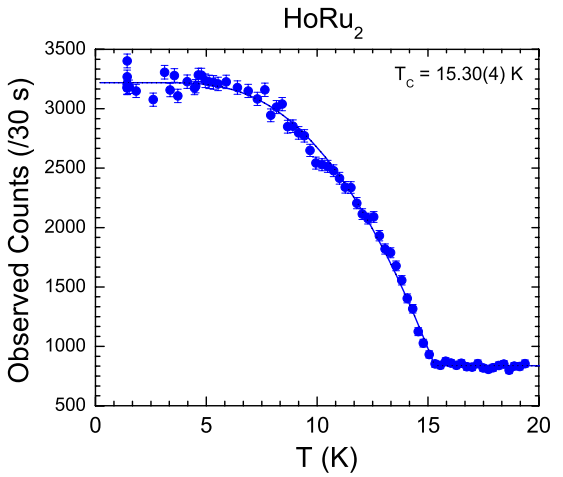

FIG. 8. (Color online) Temperature dependence of the magnetic (0,0,2) Bragg peak intensity, which yields an ordering temperature of 15.30(4) K. The intensity above the phase transition originates from the nuclear Bragg peak. Uncertainties are statistical in origin and represent one standard deviation.

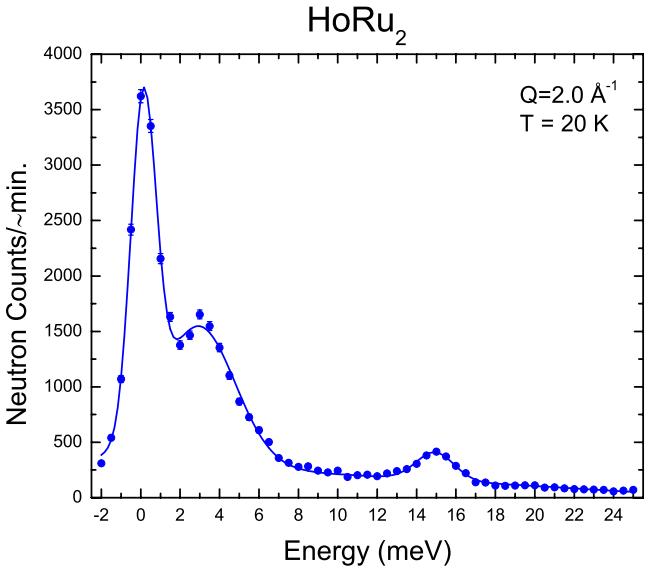

FIG. 9. (Color online) Inelastic scattering observed at 20 K and a wave vector of 2.0 $Å^{-1}$. The elastic peak has a magnetic component and nuclear incoherent scattering and is resolution limited. Two crystal field excitations are observed at 2.83(5) and 14.82(5) meV. The low energy scattering is broad, with a width of 4.34(12) meV. The energies and intensities are quite similar to the Ho crystal fields observed in cubic $Ce_{0.73}Ho_{0.27}Ru_2$ (Refs. 10 and 11).

(not shown). Contrary to the transport, magnetic, and thermodynamic data on the same sample presented in the previous section, there is no evidence of a transferred hyperfine field at the Ru sites due to magnetic order on the Gd sites.

The same apparent discrepancy between the Mössbauer spectrum and the experiments discussed above is seen in $HoRu_2$. The spectrum of $HoRu_2$ at 4.2 K is similar to that of $GdRu_2$. It is a single peak with no evidence of splitting due to a hyperfine magnetic field even though the temperature is far below the sample's Curie temperature, 15.3K.

The absence of the expected large splitting in the Mössbauer spectra in $GdRu_2$ and $HoRu_2$ points to a very small values of $B_{hyperfine}$ given that the materials are ferromagnetically ordered. This is completely different from the ruthenates where the dependence of the Mössbauer spectra reflect the internal ordered field.[14,15] In particular, $SrRuO_3$ orders ferromagnetically at 163 K and the value of $B_{hyperfine}$ is found to be 33.1 ± 1.2 T at 4.2 K. In order to get a more detailed picture of the properties of these materials we examined their electronic structure using *ab initio* calculations.

IV. ELECTRONIC STRUCTURE

The lattice parameters and structure used in the calculations for $HoRu_2$ are those given by the results of the neutron-diffraction measurements at 5 K discussed. The lattice parameters and structure were measured by Compton and Matthias (Ref. 1) for $GdRu_2$ at room temperature. However, the lattice frequently expands below a ferromagnetic transition in rare-earth intermetallic compounds.[36] So we determined lattice constants for $GdRu_2$ at low temperatures by scaling the lattice constants given by Compton and Matthias

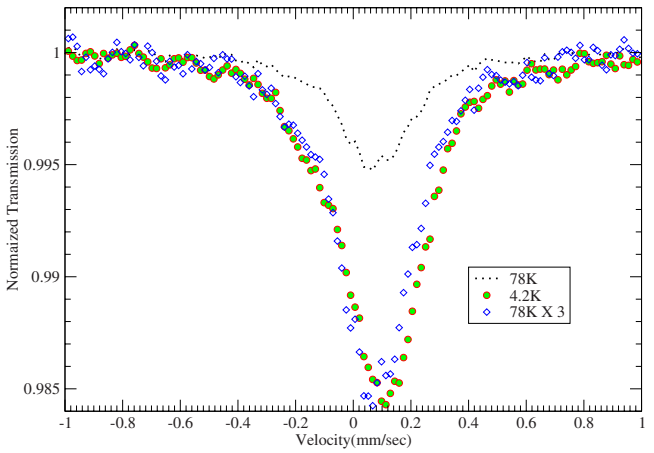

FIG. 10. (Color online) ^{99}Ru Mössbauer spectrum of $GdRu_2$ at 4.2 K (o) and at 78 K (dotted line) for a sample whose Curie temperature is 82.3 K. The 78 K spectrum ($\diamond$) is scaled by 3.0 for direct comparison with the spectrum at 4.2 K. The only temperature dependence in the spectrum between 4.2 and 100 K, based also on measured spectra at 89 and 101 K, is a continuous shift of the isomer shift to slightly more positive values. Again there is no evidence of a hyperfine magnetic field.

and found that the total energy was minimized when their values were increased by ~1%. In the analysis of the spectra there are two inequivalent Ru sites whose relative abundance is 1 to 3, in the hexagonal Laves structure ($GdRu_2$ and $HoRu_2$).

We calculated the electronic structure and the values of $B_{hyperfine}$ at the Ru and lanthanide sites using the WIEN2K software package.[27] These calculations use the LSDA, which is implemented using an extension of the augmented plane wave method. Up to 729 inequivalent $\vec{k}$ points were used in the $P6_3/mmc$ structure and RKMAX was set at 8 to ensure convergence. The energy and charge convergence variables were $ec = 10^{-5}$ Rydbergs and $cc = 10^{-5}e$. The spin on each site, S, is the net electronic spin polarization in the sphere surrounding that site.

A. Density of states and magnetic order

The calculated contributions to the densities of states in $GdRu_2$ and $HoRu_2$ show that the f bands are narrow in each case, pointing to predominantly localized states, and are split into a spin up band below E_F and a spin down band either completely ($GdRu_2$) or mostly above ($HoRu_2$), consistent with ferromagnetic order.

The calculated contributions to the density of states of $GdRu_2$ from the Gd $4f$ band and from the $4d$ bands associated with the two inequivalent Ru sites are shown in Fig. 11. The Gd spin up f band is ~4 eV below the Fermi level and spin down f band is ~1.5 eV above. The calculated value of net spin, S, on the Gd sites is 3.46 which is very close to the Hund's rule result for Gd, $\frac{7}{2}$, and to the result of the Curie-Weiss fit to the magnetic susceptibility. The calculated values of S at the two inequivalent Ru sites in $GdRu_2$ are very small, ~−0.06 and ~−0.09. The bottom two panels in Fig. 11 show the contributions to the density of states from Ru $4d$

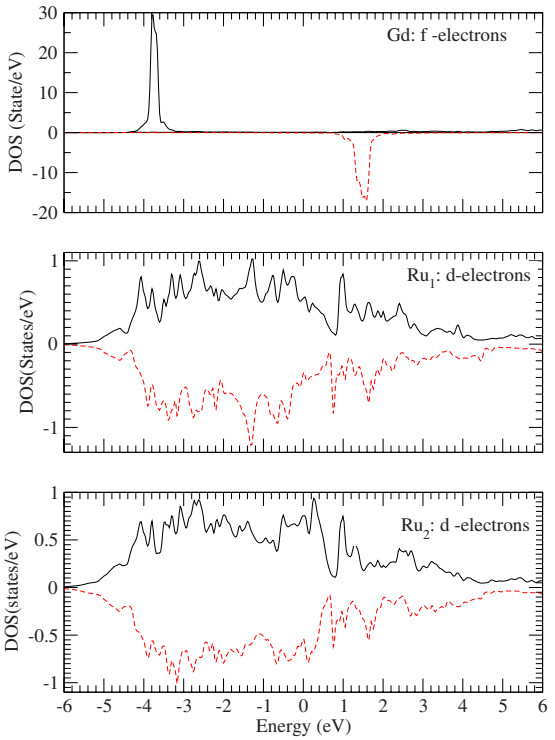

FIG. 11. (Color online) Contributions to the density of states in $GdRu_2$ derived from the narrow Gd *f*-bands and from the broad *d* bands from the two inequivalent Ru sites. Solid lines are spin up and dashed lines are spin down. $E=0$ is the Fermi level.

electrons at the two inequivalent Ru sites. $N_\uparrow$ is the contribution for states with spin parallel to the moment of the Gd site and is positive and the contribution from spin down, $N_\downarrow$, is negative for each of the inequivalent Ru two sites. At the Fermi energy the density of states is dominated by the Ru 4*d* electrons, which form broad conduction bands. The contributions from Ru 4*d* electrons, $N_\uparrow$ and $N_\downarrow$, and $N_\uparrow - N_\downarrow$ are plotted in Fig. 12 in the energy range which is 0.5 eV on either side of the Fermi energy, $E_F=0$. It is seen that the *d* electrons from both Ru sites are polarized parallel to the Gd moment with $\frac{N_\uparrow - N_\downarrow}{N_\uparrow + N_\downarrow} \simeq 0.2$ for each band arising from the two inequivalent Ru sites for energies within 0.1 eV of E_F. The total Ru *d* density of states $\sim 1.0(\text{eV Ru})^{-1}$ at $E=E_F$.

On the other hand the Gd *s* electrons have negligible weight at E_F, $\simeq 0.02(\text{eVGd})^{-1}$ and are unpolarized. This is also the case for Ru *s* electrons. This suggests that Ru *d* electrons mediate the interaction between localized Gd *f* moments. In $HoRu_2$, the Ru 4*d* Ru electrons play the same role but the minority spin band is at the Fermi energy so that it is partially occupied.

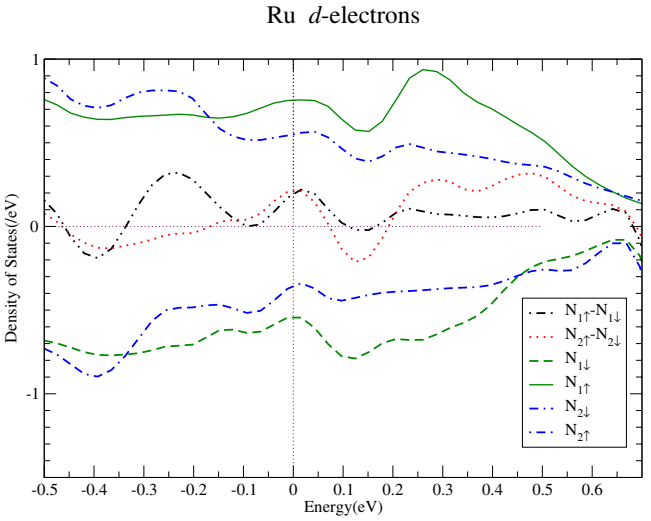

FIG. 12. (Color online) Polarization of *d* electrons from the two inequivalent Ru sites for $GdRu_2$. For both contributions there is net positive polarization at the Fermi level showing that net spin of electrons involved in scattering at low temperatures is parallel to the ordered rare earth moments. $E=0$ is the Fermi level.

In $HoRu_2$, the value of S at the Ho site is $\simeq 1.82$. This value of *S* is slightly lower than 2, the value consistent with the effective moment given by the fit to magnetic susceptibility, as determined by Hund's Rules. The absence of moments on the Ru sites in $HoRu_2$, $S \simeq 0$, is consistent with the neutron-diffraction data.

According to these results, the magnetic properties can be described by a model in which localized Gd or Ho *f* moments couple to itinerant Ru *d* electrons, rather than to itinerant *s* electrons.[24]

B. Hyperfine magnetic fields and electric field gradients

$B_{hyperfine}$ at a given site has a number of contributions which have been derived with relativistic corrections by Blügel *et al.*[37] and can be calculated directly using the WIEN2K package.[38] These contributions are the Fermi contact term, B_{con}, the dipolar field from the on-site spin density, B_{dip}, the field associated with the on-site orbital moment, B_{orb}, and the classical dipolar field from all other atoms in the system carrying moments, B_{lat}. Furthermore $B_{con}=B_{core}+B_{valence}$, where B_{core} is the contribution due to polarization of core electrons and $B_{valence}$ is the contribution from the polarization of the valence- or conduction-band electrons. These are by far the largest contributions. Powder samples are used in the experiments with small crystallites so that each Ru

TABLE II. $GdRu_2$: net electron spin, *S*, and contributions to the hyperfine magnetic fields (T) at the Gd and Ru sites.

	S	B_{core}	$B_{valence}$	B_{orb}	B_{dip}	$B_{hyperfine}$
Gd	3.46	334.55	−285.51	−2.88	−.29	49.05
Ru_1	−0.06	−4.83	0.63	−.08	0.01	−4.20
Ru_2	−0.09	−3.78	1.06	−.0.20	0.05	−2.72

TABLE III. $HoRu_2$: net electron spin, S, and contributions to the hyperfine magnetic fields (T) at the Ho and Ru sites.

	S	B_{core}	$B_{valence}$	B_{orb}	B_{dip}	$B_{hyperfine}$
Ho	1.82	179.56	−161.35	38.46	0.38	56.85
Ru_1	0.028	−1.58	−0.25	−1.82	0.04	−3.61
Ru_2	−0.009	−2.97	0.07	−0.09	−0.006	−2.99

nucleus sees the average of a collection of randomly orientated dipolar fields which presumably sum to zero. Therefore, we take B_{lat} to be zero in the current analysis.

The calculated contributions to $B_{hyperfine}$ are shown in Table II for $GdRu_2$ and in Table III for $HoRu_2$. The values of $B_{hyperfine}$ at the Ru sites are surprisingly small compared to that at the rare-earth sites in both compounds, consistent with the Mössbauer data. By comparison, the transferred hyperfine field at the Ir site in $Ir_{0.01}Fe_{0.99}$ is ~143 T compared to ~34 T at the Fe site.[20] The different contributions to $B_{hyperfine}$ on the Ru sites are all small, leading to modest values for $B_{hyperfine}$.

The values of $B_{hyperfine}$ at the Ru nuclei are also sensitive to the value of the lattice constants. In order to determine the lattice constants for $GdRu_2$ at low temperature, the electronic properties were calculated for values of the lattice constants given by Compton and Matthias (Ref. 1) scaled by a common factor, α, from 0.995 to 1.05. Although the value of the net spin on the Gd site did not change for this range of lattice constants, the hyperfine magnetic fields at the Ru sites varied from −4.49 T at $\alpha=1.00$ to 0.1 T at $\alpha=1.05$. The lowest total energy for a formula unit occurs at $\alpha=1.01$ and the values for $GdRu_2$ are calculated with this α. From Table II, $B_{hyperfine}$ at both Ru sites is negative, as one would expect from transferred hyperfine fields.[22,23]

Examining the contributions to $B_{hyperfine}$ on the rare-earth site one sees that B_{core} and $B_{valence}$ are large and of opposite sign. This is again consistent with the original discussion of Watson and Freeman.[22,23] The other contributions are negligible by comparison in $GdRu_2$. However, the magnitude of B_{orb} is ~40 T at the Ho site in $HoRu_2$. This is a substantial fraction of $B_{hyperfine}$ at that site due to the almost complete cancellation of the B_{core} and $B_{valence}$. This difference in the value of B_{orb} at the Gd and Ho sites is a reflection of the difference in the orbital angular momentum quantum number, L, on the Gd and Ho sites. Whereas Hunds' rules give $L=0$ on the Gd site because of the half-filled $4f$ shell, they give $L=6$ on the Ho site.

The electrostatic potential at a nucleus due to the surrounding charge distribution is given by the nuclear quadrupole interaction which depends on the EFG tensor at the nucleus. The calculated components of the EFG tensor for $GdRu_2$ and $HoRu_2$ are given in Table IV. The components of the EFG at each site, are small compared to those in RuO_2,[19] which also has a pure quadrupole spectrum, suggesting that each of the sites have almost cubic symmetry. In $GdRu_2$ and $HoRu_2$, the EFG are different at the two inequivalent Ru sites.

The Mössbauer spectra for these materials can now be almost completely determined with these calculated hyperfine magnetic fields and electric-field gradients. The additional parameters are the half-width half-maximum, Γ, of the absorption lines and the isomer shifts at the Ru sites. These are chosen to fit the data. The $GdRu_2$ spectrum at 4.2 K is shown in Fig. 13 and that of $HoRu_2$ in Fig. 14. The line through each spectrum is calculated with the values of $B_{hyperfine}$ and of the EFG tensors at the two inequivalent Ru sites given in Table II–IV. the non-Lorenzian shape is due to the calculated difference in the values of $B_{hyperfine}$ and EFG tensors at the two sites.

The calculations discussed here have demonstrated that it is possible for transferred hyperfine magnetic fields at the Ru sites to be very small in these ferromagnetic materials and allow us to reconcile the apparent contradiction between the results of the ^{99}Ru ME measurements and those of the transport, magnetic susceptibility, magnetization, and neutron diffraction experiments on $GdRu_2$ and $HoRu_2$.

V. DISCUSSION

A basic assumption of using the ^{99}Ru ME is that the spectrum reflects the electronic environment in the material and that magnetic order is reflected in an induced hyperfine field. However, the transferred hyperfine magnetic fields in ferromagnetic $GdRu_2$ and $HoRu_2$ are so small that one would conclude that these materials do not have magnetic order. The calculated properties of these materials have shown how this apparent discrepancy between Mössbauer and results of neutron diffraction, magnetization, transport, and specific measurements on the same samples arises. Similar calculations on other RRu_2 ferromagnets (R=Pr, Nd, Tb, Dy, and Er) for both cubic and hexagonal Laves phases, also show very small hyperfine magnetic fields on the Ru sites.[39] Analyzing the calculated contributions to $B_{hyperfine}$, the net electronic spin, S, on the Gd and Ho in Tables II and III is roughly proportional to the magnitude of the largest contributions, B_{core} and $B_{valence}$. This suggests that $B_{hyperfine}$ is almost zero on the Ru sites because S is almost zero on these sites. This arises because $4d$ Ru electrons form polarized conduction bands rather than localized moments. Consequently the ^{99}Ru ME is misleading regarding magnetic order in the RRu_2 intermetallics and, as a result, one cannot rule

TABLE IV. Diagonal elements of the electric field gradient tensor (10^{21} V/m^2) at different sites in $GdRu_2$ and $HoRu_2$.

Gd	(−1.40, −1.40, 2.79)	Ho	(−1.33, −1.33, 2.67)
Ru_1	(3.42, 3.42, −6.83)	Ru_1	(3.86, 3.86, −7.73)
Ru_2	(1.86, 0.90, −2.76)	Ru_2	(1.30, 0.93, −2.23)

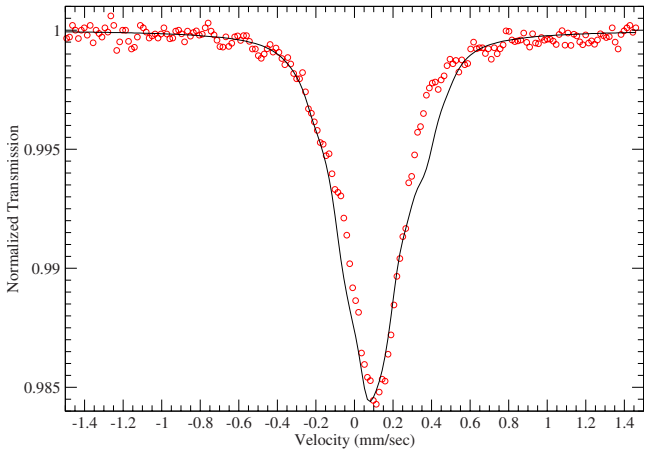

FIG. 13. (Color online) Mössbauer spectrum of $GdRu_2$ at 4.2 K (o) for a sample whose Curie temperature is 83.2 K. The solid line is the spectrum calculated with the electric field gradient components and the $B_{hyperfine}$, shown in Table II and IV. The fitting parameters are the isomer shifts at the two inequivalent Ru sites, $IS_1=0.05$ mm/sec and $IS_2=0.15$ mm/sec, and the half-width of the lines, $\Gamma=0.08$ mm/sec.

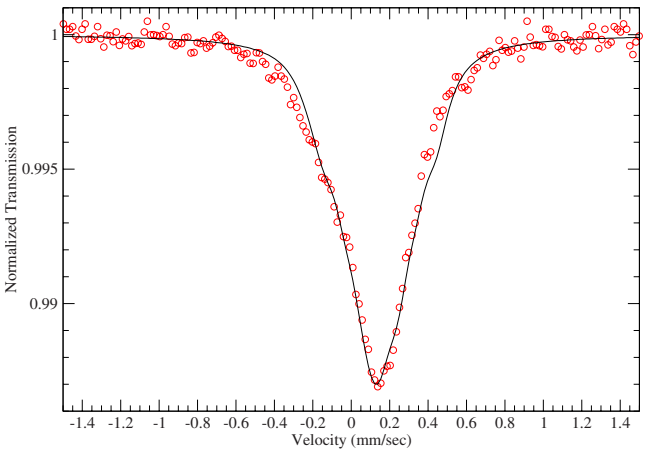

FIG. 14. (Color online) ^{99}Ru Mössbauer spectrum of $HoRu_2$ at 4.2 K. The Curie temperature is 15.3 K for this sample. The solid line is the spectrum calculated with the electric field gradient components and the $B_{hyperfine}$, shown in Table II and IV. The fitting parameters are the isomer shifts at the two inequivalent Ru sites, $IS_1=0.05$ mm/sec and $IS_2=0.18$ mm/sec, and the half-width of the lines, $\Gamma=0.08$ mm/sec.

out the coexistence of ferromagnetism and superconductivity in $Ce_{0.88}Gd_{0.12}Ru_2$ on the basis of the ^{99}Ru ME.

In contrast, moments in the magnetically ordered ruthenates are shared between Ru and O sites[40,41] and the temperature dependence of magnetic order is reflected in $B_{hyperfine}$ determined from the Mössbauer spectra. The $2p$ orbitals of the six neighboring oxygen atoms in the RuO octahedra are strongly hybridized with Ru $4d$ electrons. A possible explanation for the different behavior of Ru in the ruthenates and intermetallics lies in the difference in the electronegativities between Ru and O compared to that between Ru and rare-earth atoms. The Pauling electronegativity of oxygen atoms is 3.44, which is larger than that of Ru(2.2).[42] In $GdRu_2$ and $HoRu_2$, the opposite is the case. For Gd and Ho, the electronegativity values are 1.1 to 1.25. As a result the rare-earth atoms lose their $5d$ and two $6s$ electrons which take on the character of Ru d electrons. The nearest neighbor to each Ru atom is another Ru atom whose separation is ~2.7 Å compared to a separation of ~3.1 Å between Ru atoms and the nearest rare-earth atom. This leads to a strong competition for electrons between Ru atoms and to the wide d bands seen in the bandstucture. The structure can be pictured as a lattice of positive Gd and Ru ions, with the $4f$ moments tightly bound on the rare-earth sites as in the rare-earth metals.[43] The $4d$ derived conduction bands mediate the coupling between the rare-earth moments rather than forming localized moments on the Ru sites.

There seem to be few other examples where hyperfine magnetic fields have not been induced by magnetic order. $B_{hyperfine}$ is very small in hexagonal close-packed (hcp) Fe, which is the stable phase at high pressures. Whereas there is evidence that this phase is antiferromagnetically ordered from Raman scattering, the six-line ^{57}Fe Mössbauer spectrum disappears at the transition from bcc Fe to hcp Fe with increasing pressure.[44] $B_{hyperfine}$ was calculated by Seinle-Neumann *et al.*[45] also using the WIEN2K software. They found that there was almost complete cancellation of the large core and valence contributions to B_{con}, the Fermi contact term introduced in Sec. IV B, as the atomic volume was reduced, simulating increasing pressure. In determining the lattice constants for $GdRu_2$ at low temperature, we also found that the sign of $B_{hyperfine}$ on the Ru sites changed as the lattice constants were varied, although not at the values of interest here. However, the contributions to $B_{hyperfine}$ on the Ru sites in $GdRu_2$ and $HoRu_2$ are less than 6 T due to the itinerant nature of the $4d$ electrons.

The results of this investigation point to the unsuspected sensitivity of a nuclear probe, such as the Mössbauer effect, to the details of the electronic structure in magnetically ordered materials. The *ab initio* calculations provide a quantitative description of how the absence of the hyperfine magnetic field at the Ru site arises. In doing so, it was shown that the Mössbauer spectrum can be a probe of bandstructure, as well as the local electronic environment.

ACKNOWLEDGMENTS

Work was supported by the U. S. DOE (Grant No. DE-FG02-03ER46064) by CCSA#7669 at CSU-Fresno, and by U. S. DOE (Grant No. DE-GF02-04ER46105), and NSF (Grant No. DMR0802478) at UCSD. D.C. wishes to thank M. D. Jones of the Center for Computational Research at the University of Buffalo for his help in using the WIEN2K package.

[1] V. B. Compton and B. T. Matthias, Acta Crystallogr. **12**, 651 (1959).
[2] B. T. Matthias, H. Suhl, and E. Corenzwit, Phys. Rev. Lett. **1**, 449 (1958).
[3] A. Huxley, J. X. Boucherle, M. Bonnet, F. Bourdarot, I. Schustler, D. Caplan, E. Lelievre, N. Bernhoeft, P. Lejay, and B. Gillon, J. Phys.: Condens. Matter **9**, 4185 (1997).
[4] P. I. Kripyakevich, V. F. Terekhova, O. S. Zarechnyuk, and I. V. Burov, Sov. Phys. Cryst. (English translation) **8**, 203 (1963).
[5] M. Wilhelm and B. Hillebrand, Physica **55**, 608 (1971).
[6] K. Ruebenbauer, J. Fink, H. Schmidt, G. Czjzek, and K. Tomala, Phys. Status Solidi B **84**, 611 (1977)
[7] K. Kumagai, T. Matsuhira, and K. Asayama, J. Phys. Soc. Jpn. **45**, 422 (1978).
[8] Ø. Fischer and M. Peter, in *Magnetism: A Treatise on Modern Theory and Materials*, edited by H. Suhl (Academic Press, New York, London, 1973), Vol. V, p. 327.
[9] M. Peter, P. Donzé, Ø. Fischer, A. Junod, J. Ortelli, A. Treyvaud, E. Walker, M. Wilhelm, and B. Hillenbrand, Helv. Phys. Acta **44**, 345 (1971).
[10] J. W. Lynn and C. J. Glinka, J. Magn. Magn. Mater. **14**, 179 (1979).
[11] J. W. Lynn, D. E. Moncton, L. Passell, and W. Thomlinson, Phys. Rev. B **21**, 70 (1980).
[12] J. O. Willis, D. J. Erickson, C. E. Olsen, and R. D. Taylor, Phys. Rev. B **21**, 79 (1980).
[13] R. E. Watson and L. H. Bennett, Phys. Rev. B **15**, 502 (1977).
[14] M. DeMarco, G. Cao, J. E. Crow, D. Coffey, S. Toorongian, M. Haka, and J. Fridmann, Phys. Rev. B **62**, 14297 (2000).
[15] D. Coffey, M. DeMarco, B. Dabrowski, S. Kolesnik, S. Toorongian, and M. Haka, Phys. Rev. B **77**, 214412 (2008).
[16] G. K. Wertheim and J. H. Wernick, Phys. Rev. **125**, 1937 (1962).
[17] U. Atzmony, M. P. Dariel, E. R. Bauminger, D. Lebenbaum, I. Nowik, and S. Ofer, Phys. Rev. B **7**, 4220 (1973).
[18] H. de Graaf, R. C. Thiel, and K. H. J. Buschow, J. Phys. F: Met. Phys. **12**, 1239 (1982).
[19] O. C. Kistner, Phys. Rev. **144**, 1022 (1966).
[20] U. Atzmony, E. R. Bauminger, D. Lebenbaum, A. Mustchi, and S. Ofer, Phys. Rev. **163**, 314 (1967).
[21] D. Bosch, F. Pobell, and P. Kienle, Phys. Lett. **22**, 262 (1966).
[22] R. E. Watson and A. J. Freeman, Phys. Rev. Lett. **6**, 277 (1961).
[23] R. E. Watson and A. J. Freeman, Phys. Rev. **123**, 2027 (1961).
[24] B. D. Dunlap, I. Nowik, and P. M. Levy, Phys. Rev. B **7**, 4232 (1973).
[25] J. Callaway and C. S. Wang, Phys. Rev. B **16**, 2095 (1977).
[26] C. S. Wang and J. Callaway, Phys. Rev. B **15**, 298 (1977).
[27] P. Blaha, K. Schwarz, G. K. H. Madsen, D. Kvasnicka, and J. Lutz, WIEN2K*: Augmented Plane Wave + Local Orbitals Program for Calculating Crystal Properties* (Technische Universität Wien, Wien, Austria, 2001).
[28] P. E. Lippens, J. Olivier-Fourcade, and J. C. Jumas, Hyperfine Interact. **126**, 137 (2000).
[29] P. Blaha, K. Schwarz, W. Faber, and J. Luitz, Hyperfine Interact. **126**, 389 (2000).
[30] J. Belošević-Čavor, N. Novaković, B. Cekić, N. Ivanović, and M. Manasijević, J. Magn. Magn. Mater. **272-276**, 762 (2004).
[31] E. Pavarini and I. I. Mazin, Phys. Rev. B **74**, 035115 (2006); **76**, 079901(E) (2007).
[32] A. C. Larson and R. B. Van Dreele, Los Alamos National Laboratory Report No. LAUR086–748, 1990 (unpublished).
[33] A. Arrott and J. E. Noakes, Phys. Rev. Lett. **19**, 786 (1967).
[34] R. R. Joseph, K. A. Gschneider, Jr., and D. C. Koskimaki, Phys. Rev. B **6**, 3286 (1972).
[35] Y. Andoh, J. Phys. Soc. Jpn. **56**, 4075 (1987).
[36] S. Ohta, T. Kitai, and T. Kaneko, J. Phys.: Condens. Matter **7**, 6809 (1995).
[37] S. Blügel, H. Akai, R. Zeller, and P. H. Dederichs, Phys. Rev. B **35**, 3271 (1987).
[38] P. Novák, www.wien2k.at/reg-user/textbooks.
[39] D. Coffey (unpublished).
[40] D. J. Singh, J. Appl. Phys. **79**, 4818 (1996).
[41] I. I. Mazin and D. J. Singh, Phys. Rev. B **56**, 2556 (1997).
[42] J. Mullay, Structure and Bonding **66**, 1 (1987); *CRC Handbook of Chemistry and Physics*, edited by D. R. Lide (Taylor and Francis, London, 2005), pp. 9–77.
[43] B. Coqblin, *The Electronic Structure of Rare-Earth Metals and Alloys: The Magnetic Heavy Rare-Earths* (Academic Press, London, 1977).
[44] G. Cort, R. D. Taylor, and J. O. Willis, J. Appl. Phys. **53**, 2064 (1982).
[45] G. Steinle-Neumann, L. Stixrude, and R. E. Cohen, Proc. Natl. Acad. Sci. U.S.A. **101**, 33 (2004).